33rd Electric Vehicle Symposium (EVS33)
Portland, Oregon, June 14-17, 2020

A Microscopic Energy Consumption Prediction Tool for Fully Electric Delivery Vans

C.J.J Beckers[1], M. Paroha[2], I.J.M. Besselink[1], and H. Nijmeijer[1]
[1]*Department of Mechanical Engineering, Eindhoven University of Technology*
P.O. Box 513, 5600 MB Eindhoven, The Netherlands, e-mail: c.j.j.beckers@tue.nl
[2]*Voltia a.s., Bajkalská 5/B, 831 04 Bratislava, Slovak Republic*

Summary

For cost-optimal utilization of battery electric delivery vans, energy consumption prediction is important. This paper presents a microscopic energy consumption tool, which requires the intended route as input. Both the velocity profile prediction algorithm and the subsequent energy consumption model are based on data obtained from dedicated vehicle tests. Secondly, up-to-date environmental data on the weather, the road slope profile, and local speed legislation are obtained through API's via the internet. The results show good correspondence with the measured energy consumption. Validation with several measured trips shows that the energy consumption is predicted with an error that rarely exceeds 10 %.

Keywords: BEV (battery electric vehicle), energy consumption, medium-duty, van, efficiency.

1 Introduction

Motivated by the increasing awareness of global warming, the cargo transport sector is making a transition towards electric mobility. One example of such an electric vehicle is the Voltia eVan. The Voltia eVan is a fully electric delivery van with a swappable traction battery. Converted from a Citroën Jumper, the vehicle keeps all functional, safety, and driver-comfort features of the donor vehicle, while enhancing its driving characteristics thanks to the 160 kW (peak) electric motor. The capacity of the traction battery can vary between 40 and 90 kWh per vehicle. The Voltia eVan is also used as the carrier vehicle of a demonstrative batterypack with novel battery management system (BMS) features, which is developed within the scope of the H2020 project EVERLASTING [1].
Despite the battery capacity options and battery swapping capabilities, an accurate energy consumption prediction tool is essential for efficient utilization of these vehicles. An example of such a prediction methodology can be found in [2], where extensive fleet data is used to predict the energy consumption of electric taxi's. However, in case no large amount of fleet data is available, for instance before initial vehicle deployment, other methods are required to make accurate predictions.
In this paper, a microscopic energy consumption prediction tool for the Voltia eVan is presented. The tool consists of two parts: a velocity profile prediction (VPP) algorithm and an energy consumption prediction

Figure 1: The Voltia eVan.

(ECP) model. Both parts follow a physics-based approach in order to provide reliable extrapolation to unknown geographic regions and operating conditions. The models rely on up-to-date weather, road, and elevation data. The tool [3], developed in MATLAB, is connected via API's to OpenWeatherMap [4], OpenStreetMap [5], and the SRTM elevation map [6], respectively, to obtain these data.
The outline of this paper is as follows. In Section 2 the model and methods underlying the prediction are explained. In Section 3 the results of the energy consumption prediction tool are presented and compared to measurements. In Section 4 the results are discussed and the conclusions are presented in Section 5.

2 Methodology

2.1 Model

The energy consumption of the vehicle is modeled using a physics-based approach, i.e. by modeling the longitudinal dynamics of the vehicle, as shown in Figure 2. By applying Newton's second law we can write

$$m_{eff}\frac{dv}{dt} = F_{drive} - F_{roll,1} - F_{roll,2} - F_{aero} - F_{grav}\ . \tag{1}$$

In this equation, m_{eff} is the effective mass, which also includes rotational inertia of the wheels and driveline and v is the vehicle velocity as function of time t. Furthermore, F_{drive}, F_{aero}, F_{roll} and F_{grav} represent the driving force, aerodynamic drag force, total rolling resistance force, and longitudinal gravity component, respectively.

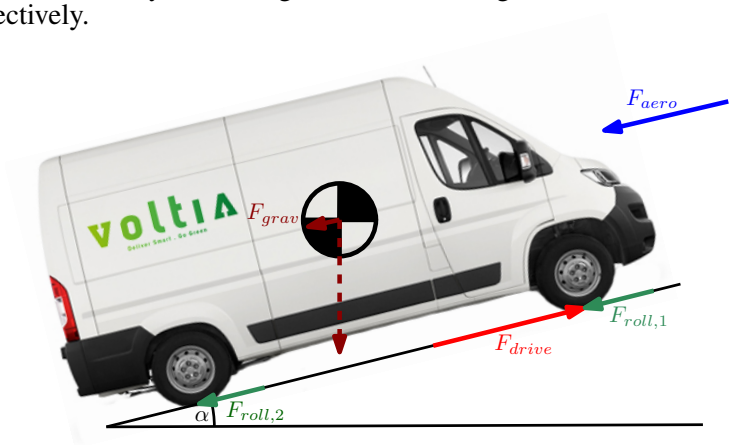

Figure 2: Schematic side-view of the Voltia eVan with all longitudinal forces indicated by arrows.

By modeling each of these forces, the power required by the powertrain P_{pt} can be calculated as [7]

$$P_{pt} = \left(m_{eff} \frac{dv}{dt} + f_r mg \cos(\alpha) + \frac{1}{2} \rho \, C_d A_f \, v_{wind,rel}^2 + mg \sin(\alpha) \right) v + P_{loss}(\omega_{wheel}, T_{wheel}) \ . \quad (2)$$

This expression is first of all a function of the vehicle velocity v. Secondly, there are several vehicle parameters, such as vehicle mass m, rolling resistance coefficient f_r, aerodynamic drag coefficient C_d, frontal area A_f, and powertrain losses P_{loss} as function of wheel speed ω_{wheel} and wheel torque T_{wheel}. Lastly, also several environmental conditions are required, such as the gravitational acceleration g, the air density ρ, the local road slope α, and the relative wind velocity $v_{wind,rel}$. The total energy consumption E_{tot} for a trip can be calculated by adding the auxiliary power P_{aux} and integrating over the trip time:

$$E_{tot} = \int_{t_0}^{t_{end}} (P_{pt} + P_{aux}) \ dt \ . \quad (3)$$

While the physics of the methodology is captured by (2) and (3) alone, the challenge lies in the accurate determination of all these vehicle and environmental parameters.

2.2 Identification of Vehicle Parameters

The model requires knowledge of several vehicle-specific parameters. Because it is generally difficult to determine these coefficients based on physical modelling alone, dedicated vehicle tests are performed.

2.2.1 Rolling Resistance and Aerodynamic Drag

Coast-down tests are performed to determine both the rolling resistance coefficient and the aerodynamic drag coefficient. During such a coast-down test, the vehicle is accelerated to a certain velocity, after which the propulsion power is removed, e.g. $P_{pt} = 0$, causing the vehicle to decelerate. By conducting this experiment on a level surface during low-wind conditions (2) reduces to

$$m_{eff} \frac{dv}{dt} + f_r mg + \frac{1}{2} \rho C_d A_f v^2 = 0 \ . \quad (4)$$

Therefore, measurement of the velocity v and its time derivative dv/dt during deceleration yields enough information to estimate both f_r and C_d, as described in [8]. Because the rolling resistance coefficient will also vary as function of road surface, the tests are repeated for different road surfaces; good asphalt, medium quality asphalt, and bad asphalt. Approximately 10 coast-down maneuvers are performed on each road surface type.
The results are displayed in Table 1 and show that the rolling resistance coefficient f_r ranges between 0.0088 and 0.0112 and increases for decreasing road quality. This road surface quality dependency is also taken into account in the energy consumption prediction. The simulation value for f_r is considered a piecewise constant function of vehicle velocity, as indicated in the last column of Table 1. The underlying assumption is that the road quality is generally better on high-velocity roads, such as highways.

Table 1: Measured average rolling resistance coefficient f_r for different road surfaces together with the applicable velocity range for usage of the value in the energy consumption prediction model.

Road surface quality	Average measured f_r [-]	Prediction velocity range [km/h]
Good asphalt	0.0088	>80
Medium asphalt	0.0092	30-80
Bad asphalt	0.0112	0-30

The aerodynamic drag coefficient is also a result of the coast-down tests. Because in theory the C_d of the vehicle does not change as function of road surface, the results of all the coast-down tests are averaged

resulting in a C_d value of 0.36. As will be explained in Section 6, information about the apparent wind yaw angle β may be available. In that case, the aerodynamic drag coefficient is considered to increase due to crosswind effects and can be calculated by

$$C_d = 0.36 + \Delta C_d\,(\beta)\ . \tag{5}$$

Here, the increase in drag coefficient ΔC_d is a function of headwind yaw angle β. Because only little research is available on the cross-wind aerodynamics of medium-duty vehicles, such as the Voltia eVan, ΔC_d is assumed to be roughly similar as for a large Multi Purpose Vehicle (MPV), as is described in [9]. Therefore, $\Delta C_d\,(\beta)$ is considered a piecewise linear function shown in Figure 3 and is assumed to be constant for $|\beta| > 10\,\text{deg}$.

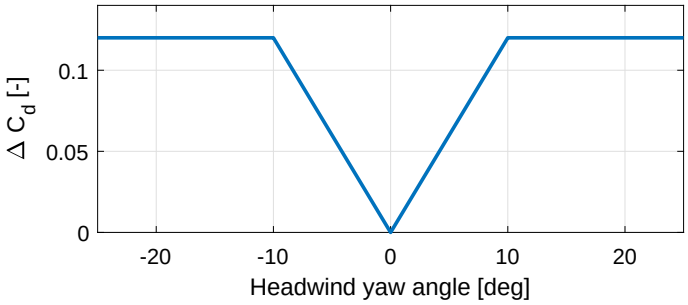

Figure 3: Increase in aerodynamic drag coefficient as function of headwind yaw angle.

Lastly, the vehicle mass is determined by weighing the empty vehicle and adding the mass of the cargo and drivers, resulting in $m = 2800\,\text{kg}$. Additionally, the effective mass is calculated based on the known inertia of the tires and motor rotor, resulting in $m_{eff} = 2880\,\text{kg}$.

2.2.2 Powertrain Losses and Regenerative Braking

The powertrain loss P_{loss} is difficult to determine based on physical modeling. This term represents all the power lost between the vehicle's traction battery and the wheels, and includes both electrical losses in the inverter and motor, as well as mechanical losses in the gearbox, bearings, and driveshafts. Therefore, the choice is made to measure the lumped powertrain losses using vehicle tests.

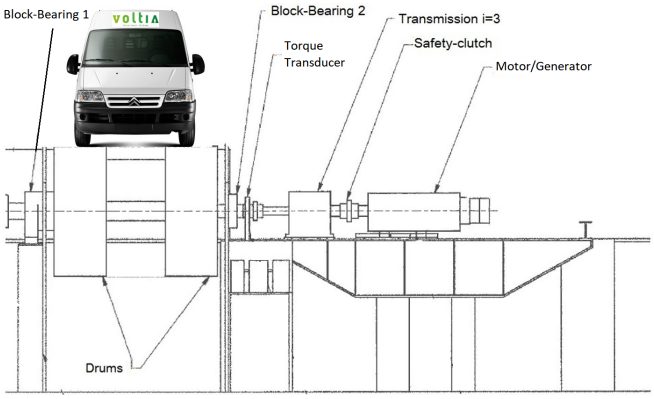

Figure 4: Schematic view of the Voltia eVan placed on the TU/e Heavy Duty Chassis Dynamometer.

The TU/e Heavy Duty Chassis Dynamometer, displayed in Figure 4, allows for the measurement of the mechanical power output at the driven wheels of the vehicle P_{wheel}. Simultaneously, the electrical power P_{DC} at the DC-side of the vehicle's powertrain inverter is measured. This way, the powertrain losses can be determined as

$$P_{loss} = P_{DC} - P_{wheel}\ . \tag{6}$$

By operating the vehicle in steady-state at several combinations of velocities and torques, the powertrain loss is mapped for the entire operating range of the powertrain. The results are visualised as efficiency values in Figure 5a, and represent the efficiency of the inverter, motor, gearbox, and axle combined. The efficiency is calculated separately for the driving situation η_{drv} and the regenerative braking situation η_{brk}:

$$\eta_{drv} = \frac{P_{wheel}}{P_{wheel} + P_{loss}} \qquad \eta_{brk} = \frac{|P_{wheel}| - P_{loss}}{|P_{wheel}|} \,. \tag{7}$$

The measured powertrain losses are implemented in the energy consumption prediction algorithm as P_{loss} in (2) and are considered to vary as function of wheel angular velocity ω_{wheel} and wheel torque T_{wheel}.

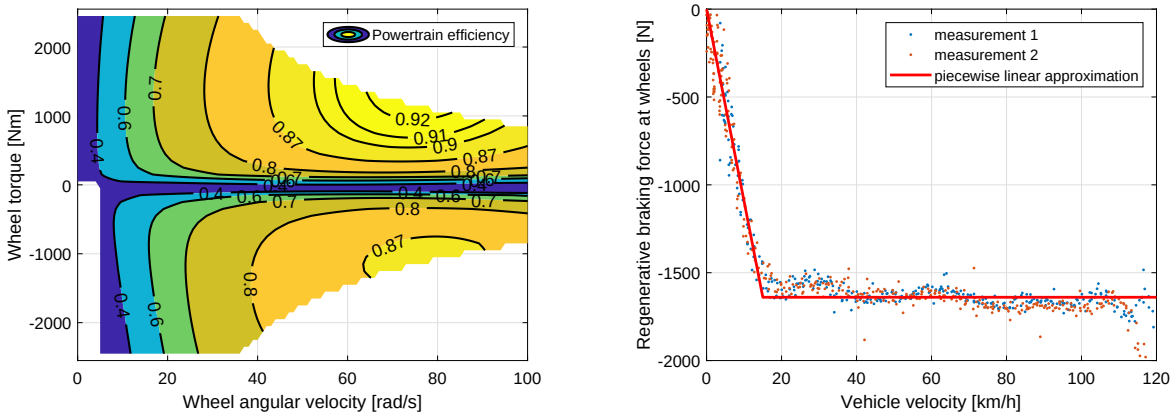

(a) Powertrain efficiency from battery to wheels.

(b) Maximum regenerative braking force.

Figure 5: Results of the TU/e Heavy Duty Chassis Dynamometer tests.

Furthermore, coast-down experiments are conducted on the dynamometer with the goal of identifying the regenerative braking characteristics of the vehicle. The moment of inertia of the dynamometer is known, thus the braking force exerted by the vehicle on the drum can be determined during such a coast-down test. The results are displayed in Figure 5b and show a regenerative braking force that is approximately constant, except at lower velocities. In the energy consumption prediction model this force is modeled by a piecewise linear function, also indicated in Figure 5b. During normal operation of the vehicle the applied braking force up until this piecewise linear function is assumed to be regenerative. Any additional braking force exceeding this limit is applied using the hydraulic friction brakes and is therefore excluded from the regenerative braking gain. Lastly, the auxiliary power is considered to be constant based on measurements, resulting in $P_{aux} = 650\,\text{W}$.

2.3 Identification of Environmental Parameters

The longitudinal dynamics model in (2) requires knowledge of several environmental parameters. While some of these parameters are universal constants, such as the gravitational acceleration $g = 9.81\,\text{m/s}^2$, others might vary as function of location and/or time. Therefore, relevant information is obtained for an arbitrary route through use of online Application Programming Interfaces (API's).

2.3.1 Road Slope

The local road slope α is determined from the SRTM elevation database [6]. By making use of the `readhgt` toolbox [10] relevant sections of the digital elevation map are downloaded and queried. The resulting elevation, as function of travelled distance, is filtered by a 3$^{\text{rd}}$ order Butterworth low-pass filter with cut-off spatial frequency $\lambda_c = 1/2000\,\frac{1}{\text{m}}$, and differentiated numerically to obtain the local road

gradient α, see Figure 6. This specific λ_c indicates that all features smaller than approximately 2 km are filtered out of the elevation profile. This step is essential, as otherwise short wave length variations in the elevation map will result in unrealistic road gradients, which can severely impact the accuracy of the energy consumption prediction.

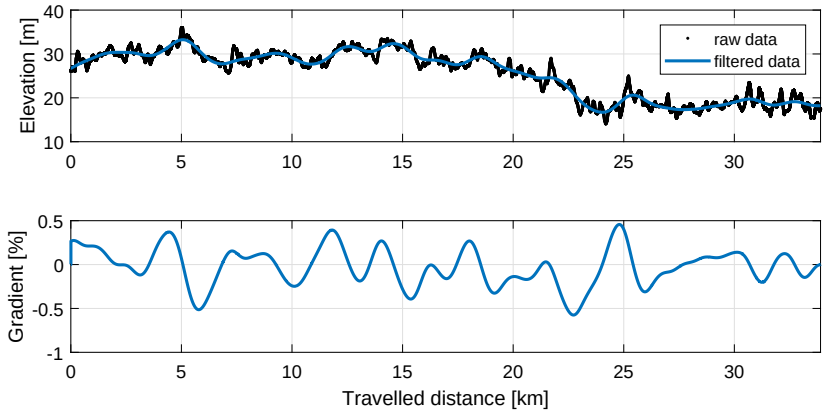

Figure 6: Elevation and gradient for one of the driven routes with the Voltia eVan.

2.3.2 Weather Data

The energy consumption prediction algorithm takes up-to-date weather information into account. To this end, temperature T, air pressure p_a, wind magnitude, and wind direction are obtained from OpenWeatherMap [4]. The temperature and air pressure are used to calculate the air density $\rho(T, p_a)$ [11].

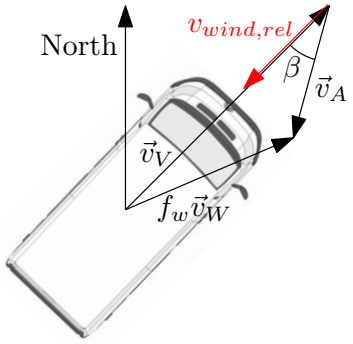

Figure 7: Top view of the Voltia eVan with the vehicle velocity vector $\vec{v}_V$, the scaled wind velocity vector $f_w\vec{v}_W$, the apparent wind vector $\vec{v}_A$ and the relative longitudinal wind velocity $v_{wind,rel}$.

The wind magnitude and direction are represented by the vector $\vec{v}_W$, which indicates the direction the wind is blowing towards with respect to the north. This vector is used together with the vehicle velocity vector $\vec{v}_V$, whose direction is calculated from the vehicle heading, to determine the apparent wind vector $\vec{v}_A$

$$\vec{v}_A = f_w\vec{v}_W - \vec{v}_V \ , \tag{8}$$

which is also depicted in Figure 7. Practise shows that it is beneficial for the energy consumption prediction to scale the wind magnitude by choosing the constant factor $f_w < 1$. This factor is also used to compensate for the fact that the obtained wind magnitude is specified at an altitude of 10 m above the road surface instead of 1 m, where the vehicle drives. To compensate for this altitude difference an f_w of approximately 0.28 is expected [12, p. 56]. For the result presented here, $f_w = 0.2$ was used, because it results in the most accurate predictions for the analysed trips. The reason is that $f_w < 0.28$ is that the vehicle rarely drives in an open field where it is subject to the full influence of the wind. More often

the vehicle is sheltered from the wind by road-side structures, trees, or buildings. As last step, the apparent wind direction β is calculated, which is used to determine $\Delta C_d(\beta)$ as described in Section 2.2.1. Furthermore, β is used to calculate the relative longitudinal wind direction $v_{wind,rel}$

$$v_{wind,rel} = |\vec{v}_A| \cos(\beta) \ , \tag{9}$$

which is used in (2).

2.4 Prediction of the Velocity Profile

The expression in (2) also requires knowledge of the velocity profile of the vehicle. A velocity predicting algorithm is developed, based on [7], that requires GPS coordinates of an intended route as input.
By use of the `OpenStreetMap Functions` toolbox [13], the algorithm queries relevant road information from OpenStreetMap [5]. This includes the local speed legislation and traffic sign locations. The information is visualised in Figure 8 for the route that will also be discussed in Section 3.

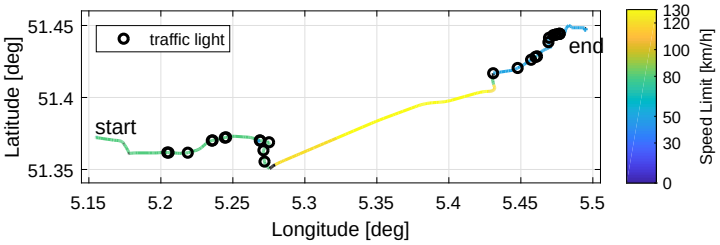

Figure 8: Legislated maximum velocity and traffic sign location according to OpenStreetMap.

In the first step of the velocity profile prediction, the local speed legislation is considered to dictate the maximum velocity along the route. Next, further velocity constraining locations are identified. These include traffic light locations and corners. The vehicle is assumed to make a full stop at every encountered traffic light. The reduced velocity in a corner is a function of the corner curvature calculated using the GPS-points and an assumed maximum lateral acceleration of $2\,\mathrm{m/s^2}$. The result is a profile dictating the upper-bound of the velocity v_{max} as function of travelled distance s, which is discretized as

$$s = [s_1, s_2, ..., s_i, ..., s_N] \quad \text{for} \quad i = 1, 2, ..., N \ , \tag{10}$$

where N is the total number of coordinates along the route.

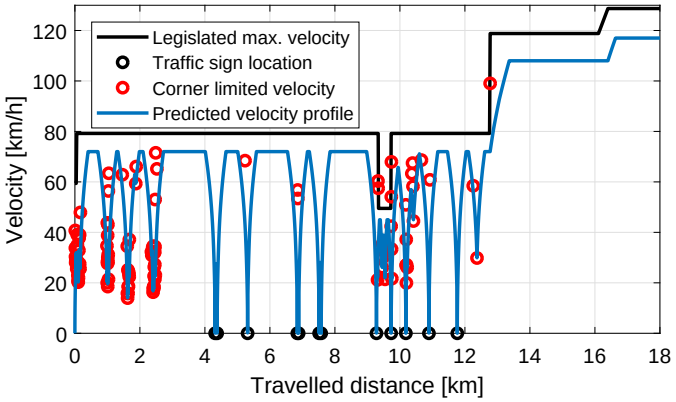

Figure 9: Detail of the determined velocity constraining locations and the resulting predicted velocity profile.

The final velocity profile is determined by including a limited vehicle acceleration and deceleration. Because these limits are mainly dictated by the driver, they are referred to as the driver model. The preferred cruising velocity is also assumed to be driver specific and is calculated as factor of the legislated maximum velocity. The three driver specific parameters; acceleration, deceleration, and cruising velocity, are tuned based on recorded data to represent the average driving behavior of a particular driver, as shown in Figure 10a.
In order to include the acceleration limit, numerical time integration is performed in between each of the points of the distance grid s, while also taking the upper-bound of the velocity v_{max} into account:

$$v(s_{i+1}) = \min \left(\int_{t(s_i)}^{t(s_{i+1})} a_{x,lim}(v)dt + v(s_i) \ , \ v_{max}(s_{i+1}) \right) \quad \text{for} \quad i = 1, 2, ..., N-1 \ , \qquad (11)$$

where $a_{x,lim}$ is the acceleration limit, displayed in Figure 10a. This procedure is performed once in forward direction, as shown in (11), and once in backward direction, to include the deceleration limit. Using the now known velocity, the velocity profile as function of distance is interpolated to a time grid. The resulting velocity profile Figure 10b shows a fair correspondence with a measured velocity profile.

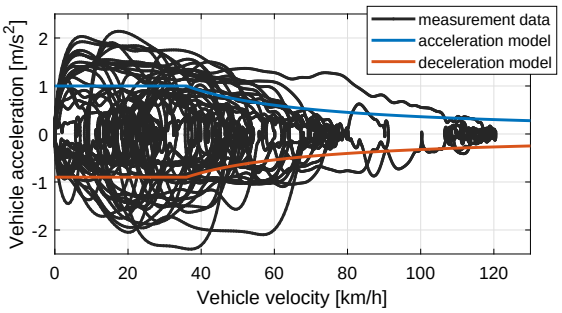

(a) Measured and modeled vehicle acceleration.

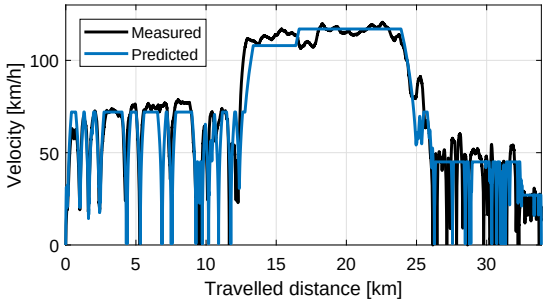

(b) Measured and modeled velocity profile.

Figure 10: Driver model that is used as input for the velocity profile prediction (a) and the resulting predicted velocity profile (b), both compared to measured data (black).

The prediction algorithm contains multiple assumptions, such as the completely deterministic driver model, and the fact that the vehicle stops at every traffic light. Even though not all realistic details are represented, the resulting velocity profile is accurate enough for the goal of energy consumption prediction.

3 Energy Consumption Prediction Results

Having knowledge about the velocity profile and the vehicle and environmental parameters, the energy consumption can be predicted for a given route. To this end, the velocity profile is first predicted, as described in Section 2.4. The predicted velocity profile $v(t)$ is then used as input for (2) and (3), together with all the parameters described in Section 2.2 and 2.3.
In order to validate both parts of the model, a comparison with measured data is made. A 33.9 km route is used as input. Data for the same route are also displayed in Figures 6, 8, 9, and 10. First of all, the energy consumption model is validated by using the measured velocity, also shown in Figure 10b as input to (2) and (3). The results, displayed in Figure 11a, show a good correlation between model and measurement, except for a slight under-estimation of the regenerated energy.

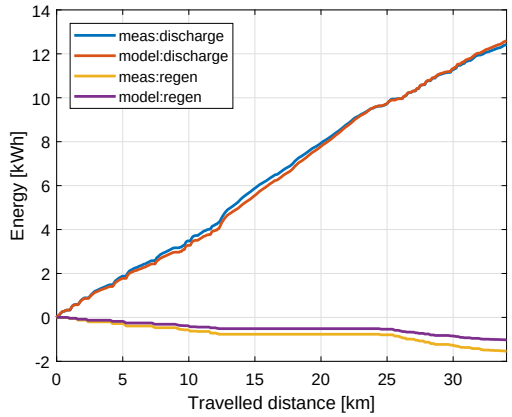

(a) Predicted energy based on measured velocity.

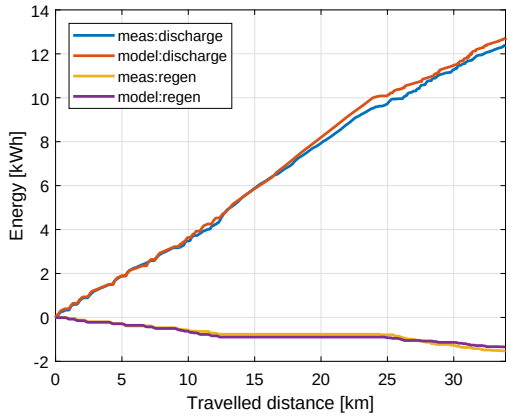

(b) Predicted energy based on predicted velocity.

Figure 11: Predicted energy consumption compared to the measured energy consumption. In (a) the measured velocity $v(t)$ was used, whereas in (b) the predicted velocity profile was used.

Next, the same calculations are performed by taking the predicted velocity profile, shown in Figure 10b, as input for the energy consumption model. The result is presented in Figure 12, which displays the power described by each of the terms in (2) as function of time. Integrating and summing these powers, results in the total energy displayed in Figure 11b. The result shows a correct estimation of the regenerated energy and a slight over-estimation of the dissipated energy. Ultimately, the difference between the measured and predicted energy consumption at the end of the trip is 4.3%.

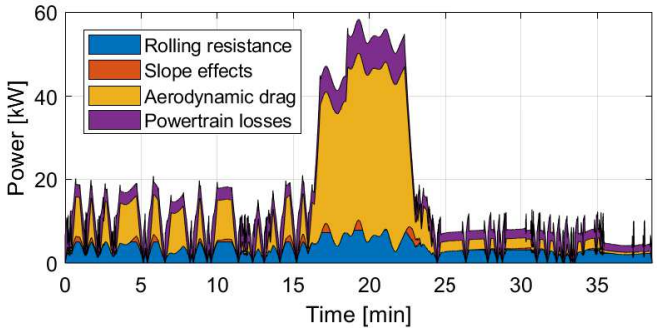

Figure 12: Overview of the power lost due to each of the terms in (2).

The results of several trips are listed in Table 2. All trips are conducted in and around the city of Eindhoven, the Netherlands. The longer distance trips, e.g. trip 1, 3 and 4, include highway driving. All trips contain city driving. Based on five analysed trips with an average length of 17.6 km, the tool is fairly accurate and stays mostly below 10 % with respect to the measured energy consumption. Trip number 5 is an exception. Most probably, the rolling resistance coefficient described in Section 2.2.1 is not in accordance with the real type of road along this short route.

Table 2: Results of the energy consumption prediction tool for five different trips. Data from Trip 4 is detailed in other figures throughout this paper.

	Distance [km]	Measured Energy [kWh]	Predicted Energy [kWh]	Error [%]
Trip 1	16.2	3.9	3.7	−5.3
Trip 2	6.8	1.5	1.4	−8.6
Trip 3	29.7	9.2	10.0	8.9
Trip 4	33.9	10.9	11.3	4.3
Trip 5	1.7	0.3	0.4	12.0

4 Discussion

In theory, the model includes the influence of road slope and wind in the energy consumption. However, because the validation sets were recorded in the Netherlands during relatively low-wind conditions of $|\vec{v}_W| \leq 3$ m/s, the model should still be validated for more extreme situations.
Analysis of the predicted trips also shows that traffic can have a significant influence on the velocity profile and consequently on the energy consumption. Because at the time of writing, no free up-to-date traffic data was available, this effect is not included in the tool. Nevertheless, including information related to the traffic flow would probably increase the accuracy of the velocity profile and thus the energy consumption prediction.
Furthermore, the energy consumption prediction depends on several tunable parameters, such as f_w, λ_c and the chosen acceleration limits that capture the driver behavior. These are typically tuned based on measured data from an arbitrary route. Therefore, some vehicle data and knowledge related to the driver behavior will always be beneficial to get a good prediction accuracy for future trips.

5 Conclusions

The microscopic energy consumption prediction tool can be used for any predetermined route and shows a fair correspondence with the available measurements. For most of the analysed trips the deviation between predicted and measured energy consumption stays below 10%.
During development of the tool, it was concluded that the most accurate results are obtained by only partially taking the wind speed into account and that filtering the STRM elevation profile is important. Validation of the tool with more extreme slope and weather conditions is considered future work. However, decent extrapolability is expected, based on the usage of a physical model and up-to-date map data. The full MATLAB-code for the tool, including connection to the aforementioned API's is freely available in [3].

Acknowledgments

The code of the tool is partially built upon the work of [14]. This contribution is gratefully acknowledged. This project has received funding from the European Unions Horizon 2020 research and innovation programme under grant agreement No. 713771.

References

[1] EVERLASTING Consortium. Everlasting project website. `https://everlasting-project.eu/`. [Accessed on: 2020-03-20].

[2] Anthony Deschênes, Jonathan Gaudreault, and Kim Rioux-paradis. Predicting electric vehicle consumption: a physical model that fits. In *32nd Elec. Veh. Symp. (EVS32)*, Lyon, France, 19-22 May 2019.

[3] C.J.J. Beckers, T.A.G.H. Geraedts, Igo J. M. Besselink, and Henk Nijmeijer. Matlab-scripts describing a microscopic energy consumption prediction tool for electric vehicles. 4TU.Centre for Research Data, April 2020. URL https://dx.doi.org/10.4121/uuid:721b2ea6-2634-4dd5-a0c8-865a0aa41a99.

[4] OpenWeather ®. Openweathermap. https://openweathermap.org/current.

[5] © OpenStreetMap contributors. Openstreetmap. https://www.openstreetmap.org/copyright.

[6] Tom G. Farr et al. The shuttle radar topography mission. *Rev. Geophys.*, 45(2):RG2004, May 2007. https://www2.jpl.nasa.gov/srtm/.

[7] Jiquan Wang, Igo Besselink, and Henk Nijmeijer. Battery electric vehicle energy consumption prediction for a trip based on route information. *Proc. Inst. Mech. Eng. Part D J. Automob. Eng.*, 232(11):1528–1542, September 2018.

[8] NEN-ISO Standard. Road vehicles - Road load - Part 1: Determination under reference atmospheric conditions. Technical Report 10521-1:2006 en.

[9] Jeff Howell. Aerodynamic Drag of Passenger Cars at Yaw. *SAE Int. J. Passeng. Cars - Mech. Syst.*, 8(1):2015–01–1559, April 2015.

[10] François Beauducel. Franois beauducel (2020). readhgt: Import/download nasa srtm data files (.hgt) (https://www.mathworks.com/matlabcentral/fileexchange/36379-readhgt-import-download-nasa-srtm-data-files-hgt). MATLAB Central File Exchange, 2020. [Retrieed March 2, 2020].

[11] A. Picard, R. S. Davis, M. Gläser, and K. Fujii. Revised formula for the density of moist air (CIPM-2007). *Metrologia*, 45(2):149–155, apr 2008.

[12] T. R. Oke. *Boundary Layer Climates*. Routledge, London, UK, 2 edition, September 2002.

[13] Ioannis Filippidis. Openstreetmap functions (https://github.com/johnyf/openstreetmap). Github, 2016. [Retrieved March 2, 2020].

[14] T.A.G.H. Geraedts. Programming of an energy consumption prediction algorithm for an electric vehicle. BSc thesis, DC 2019.071, Eindhoven University of Technology, Eindhoven, 2019.

Authors

Camiel Beckers is a PhD student in the Department of Mechanical Engineering at Eindhoven University of Technology (TU/e) since 2017. He obtained his master's degree at the same university, working on bifurcation theory to faster simulate shimmy in aircraft landing gear. His current research interests include energy consumption modeling of battery electric vehicles, with a focus on electric city buses.

Mário Paroha is the head of R&D at the electromobility company Voltia. He is also responsible for international R&D collaborations of the company. He has an academic background in electrical engineering and has gained expertise in different companies and institutions. This includes the design of ultrasound sensors in Austria and testing of optoelectronic elements in Belgium. His interests include electric vehicles, charging infrastructure and new business models.

Igo Besselink is an Associate Professor and Chair of Vehicle Dynamics in the Department of Mechanical Engineering at Eindhoven University of Technology (TU/e). His key area of expertise is Vehicle Dynamics: the analysis of road vehicle motions, vibrations and stability as a result of steering, driving, braking and external disturbances. Igo's main research interests are aerodynamics of commercial vehicles, tire behavior and modeling, battery electric vehicles and vehicle control.

Henk Nijmeijer is a Full Professor at Eindhoven University of Technology (TU/e) and Chair of the Dynamics and Control group. Henk's research focuses on Control Systems Engineering, Mechanical Engineering and Automotive Engineering. His areas of expertise include (advanced) control theory and systems, robotics, mechatronics, (system) dynamics and control systems engineering.